# AN INNOVATIVE NEW CELL FOR TESTING ROCK CORE UNDER TRUE TRIAXIAL STRESS STATES

**B.G.D. SMART, B.R. CRAWFORD**

DEPARTMENT OF PETROLEUM ENGINEERING
HERIOT-WATT UNIVERSITY

## ABSTRACT

This paper describes the design of a unique new cell developed specifically for the testing of cylindrical core plugs under general 3-D stress, $\sigma_1 \neq \sigma_2 \neq \sigma_3$, truly representative of *in situ* conditions. The test procedure is similar to the conventional axisymmetric triaxial test, with the maximum principal stress being applied axially to the rock specimen via a stiff, servo-hydraulic compression rig. The innovation lies in application of radial pressure to the sample circumference, which is achieved through hydraulic pressurisation of twenty four "trapped tubes" aligned with the specimen long axis, and trapped between its jacketing sleeve and the cell wall. Coupling of opposing banks of these tubes into different servo-controlled hydraulic circuits enables a differential confining pressure to be applied to the specimen circumference. This relatively simple design eliminates the need for complex sample geometries such as the traditional cubic specimen or hollow cylinders, and as such is ideal for routine core analysis. Initial testing utilising the true triaxial cell and its computer control and data acquisition facility, indicates that the intermediate principal stress has a strong influence on the deformation, strength and permeability characteristics of a Rotliegend reservoir sandstone analogue. It is suggested that the cell has the potential for widespread application in the petroleum industry as a cost-effective means of factoring stress and permeability anisotropy into calculations.

## INTRODUCTION

The *in situ* stress field is conventionally characterised by the magnitudes and directions of the three principal stresses, $\sigma_1 > \sigma_2 > \sigma_3$. For essentially flat-lying reservoir sediments with the earth's surface acting as a free-boundary, one principal stress (normally $\sigma_1$) will be vertical and equal to the net overburden, $\sigma_v$, derived by integration of the formation density compensated log, so that the other two principal stresses (normally $\sigma_2$ and $\sigma_3$) must be horizontal. In tectonically inactive areas these two stresses can be considered approximately equal, however for the more general case, $\sigma_H > \sigma_h$, the formation breakdown pressure and the instantaneous shut-in pressure derived from hydraulic fracturing give indications of $\sigma_2$ and $\sigma_3$ respectively. Phenomena such as borehole breakout and azimuthal trends between injecting and producing wells testify to pronounced horizontal stress anisotropy. Such stress anisotropy has a direct influence on the orientations of both natural and production induced fractures which can act either as pronounced fluid conduits (dilatant joints) or as fluid barriers (sealing faults). Also, the *in situ* stress state can result in permeability anisotropy of the intact rock matrix, particularly within stress-sensitive reservoir sandstones.

For competitive planning, exploitation and management of hydrocarbon reservoirs, reliable permeability estimates are a prerequisite. Laboratory measurements on recovered core must therefore seek to reproduce the *in situ* environment as closely as possible, to allow confident extrapolation to the field, however, routine core analysis is normally performed under conditions of hydrostatic external stress. One factor which has largely been ignored with regard to reproduction in the laboratory, is a realistic 3-D general triaxial stress field. Experimental equipment designed for the application of polyaxial stresses has, to date, proved essentially unsuitable for routine core analysis involving quantification of the effects of such stresses on deformation, strength and permeabiltity. To address this

deficit, a new true triaxial cell has been designed which is capable of testing plugs taken from reservoir whole core. Experimentation with the cell indicates that the effects of applying a truly realistic 3-D stress state are of first order significance.

## PREVIOUS EXPERIMENTATION

### Conventional Triaxial Testing

Non-hydrostatic stress states are routinely imposed on core plugs during rock mechanical laboratory testing. In such conventional "triaxial" tests, a uniform radial stress is applied by fluid pressure to the curved surface of a rock cylinder, whilst simultaneously the prepared flat and parallel specimen ends are loaded axially through spherical seats and platens. The radial pressure or confinement is usually achieved using a "Hoek and Franklin-type cell"[1, 2] in which hydraulic fluid at pressure p, acts on a synthetic rubber membrane sheathing the sample. Ideally, the axial load is applied parallel to the cylindrical specimen long axis via a stiff, servo-hydraulic controlled compression rig. Axial loading over the specimen cross-sectional area in this manner results in an axial stress $\sigma_a$, wholly independent of p.

Independent control of only $\sigma_a$ and p, combined with the geometrical constraints inherent in the above system, results in two admissable stress field conditions which are within the limitations of conventional "triaxial" testing capabilities. In the "triaxial" *compression* test the specimen is subjected to an axial stress equal to the maximum principal stress, $\sigma_a=\sigma_1$, whilst the uniform-radial confinement is set lower giving $p=\sigma_2=\sigma_3$ ($\sigma_2$ and $\sigma_3$ being the intermediate and minimum principal stresses respectively). Hydraulic cell pressure p is usually held constant whilst the axial stress $\sigma_1$ is increased until the specimen ruptures. In the alternative and less common "triaxial" *extension* test, rupture is achieved by increasing p or decreasing $\sigma_a$, in both cases the hydraulic cell pressure being higher than the axial stress in the specimen. This gives rise to the stress state $\sigma_1=\sigma_2=p>\sigma_3$ where $\sigma_3$ is the axial stress. Although $\sigma_3$ is compressive, in this case the axial *strain* is tensile for small $\sigma_3$, causing an increase in specimen length.[3]

For both the "triaxial" compression and extension tests described above, it is evident that two of the three principal stresses are equal at any one time, and that for tests utilising a uniform-radial hydraulic pressure cell, the applied stress fields represent special cases of a general 3-D or true triaxial stress state in which all three principal stresses are unequal and independent, $\sigma_1\neq\sigma_2\neq\sigma_3$. In the preceding discussion, triaxial is quoted in inverted commas to impress that either $\sigma_2=\sigma_3$ (compression) or $\sigma_1=\sigma_2$ (extension) test configurations are specified. Henceforth such stress distributions wil be rigorously referred to as "axisymmetric triaxial" to avoid confusion with the general case. Thus the two conditions admissable under axisymmetric triaxial testing are $\sigma_1>\sigma_2=\sigma_3$ and $\sigma_1=\sigma_2>\sigma_3$. The importance of these two variations of the axisymmetric triaxial test is that they represent the lower and upper bounds respectively of the intermediate principal stress, and as such can be used to investigate its influence in particular upon rock failure.

Brace[4] performed axisymmetric triaxial compression and extension tests to failure on dolerite, dolomite, granite and quartzite specimens, which showed no significant variation between the results obtained when $\sigma_2=\sigma_3$ and when $\sigma_2=\sigma_1$. Whilst these tests included the maximum possible variation of $\sigma_2$ between $\sigma_3$ and $\sigma_1$, from which the obvious conclusion was that its magnitude had a negligible influence on rupture strength, the axisymmetric configuration precluded any extrapolation to the effects of a general triaxial stress field on the failure strength of these lithologies.

### Polyaxial Testing of Cubic Specimens

In order to experimentally assess the effects of a truly general triaxial stress field on rock strength, to date workers in this field have adopted the experimental setup whereby three independently variable principal stresses are applied to opposing faces of cubic rock specimens. This configuration is the only one capable of maintaining a

uniform and homogeneous stress state in the specimen, over all combinations of principal stresses sufficient to cause rupture. The *polyaxial* (synonymous with *multiaxial* or *true triaxial*) test as it is known, has been applied almost exclusively to study the effect of $\sigma_2$ on rock strength, to map out failure surfaces in 3-D stress space and to formulate generalised constitutive laws for various geomaterials.

Hojem and Cook[5] carried out tests using a polyaxial cell in which small flat jacks were used to subject rock cubes to a true triaxial stress state, and formulated an effective shear strain energy failure criterion[6] based on the resultant data, which showed that $\sigma_2$ had a first order effect on rock strength. Mogi[7, 8, 9] tested cubic samples from a variety of lithologies and found more significant strength differences than had been reported by Brace or by Hojem and Cook. The impact of his results are summarised by Scholz[10]. Mogi showed that under true triaxial stress, as $\sigma_2$ was increased above $\sigma_3$ to $\sigma_1$, microstructural deformation was such that: dilatancy occurred by the opening of microcracks in the $\sigma_3$ direction; cracking formed preferentially in the $\sigma_1$, $\sigma_2$ plane; the degreee of induced anisotropy was controlled by the principal stress ratios. With regard to macroscopic strength he showed that: the increase in strength as $\sigma_2$ was increased from $\sigma_3$ to $\sigma_1$ was less than if $\sigma_2$ and $\sigma_3$ were increased in step; the macroscopic fracture formed at an acute angle to $\sigma_1$ and parallel to $\sigma_2$ in accordance with the Coulomb criterion; the minimum lateral dilatancy direction was parallel to the strike of the fracture plane. Thus the polyaxial testing conducted by Mogi showed macroscopic shear failure to be markedly dependent on both the magnitude and orientation of $\sigma_2$. Increasing $\sigma_2$ was observed to suppress dilatancy causing the rupture strength to increase. Fracture orientation was observed to be controlled by the dominant orientation of induced microcracks, which in turn was largely controlled by the applied stress ellipsoid. However, Hoek and Brown pointed out that Mogi's data suggested that many of his tests involved brittle/ductile transitions, which would have a resultant effect on any interpretation.

More recent polyaxial test data from cubic specimens includes that of Gau *et al* [11], who tested 10-cm red sandstone cubes loaded by both rigid and flexible platens, Amadei and Robinson[12], who tested limestone under conditions of combined compression and tension with flexible fluid-filled and brush platens respectively, and Esaki and Kimura[13], who used a high pressure true triaxial box with rigid platens to apply stresses into the Gigapascal range whilst monitoring acoustic emissions. All the above demonstrated that the magnitude of $\sigma_2$ has an important effect on rock strength.
Sture and Desai[14] pointed out that whether the forces are applied to the specimen through flexible membranes or via rigid platens has a great effect on the distribution of stresses and strains within the rock cube. Whilst flexible membranes ensure uniform loading distributions normal to the loading faces, and rigid platens ensure accurate measurement of strains and the application of higher stress fields, the uniformity of stresses induced by the latter system is doubtful.

Jaeger and Cook[15], list various references on the testing of ceramic materials which can be obtained in the form of thin-walled cylinders, the geometry of which ensures that the various criteria for failure can be studied under a wide range of (approximately) homogeneous stresses. Handin *et al* [16] utilised the method for rock testing, applying torsion to hollow cylindrical specimens of limestone, dolomite and glass under $\sigma_a$ and p to obtain true triaxial stress states.

Considering that *in situ* stress distributions are inherently 3-D, the need for generalised triaxial testing to develop numerical methods and constitutive laws has never been greater. However, the polyaxial testing methods detailed above are far removed from being ideal as routine experimental procedures for providing reliable data. With particular regard to petroleum-related rock mechanical requirements, existing methods of polyaxial rock testing are especially extraneous due to:

(i) the relatively large size of specimens required from "valuable" whole core, as such sampling would be in direct competition with plugging for petrophysical evaluation. Also, the complex geometry of specimens (cubes and thin-walled cylinders) poses problems with respect to weak reservoir sandstones and shales.

(ii) Difficulties involved with the testing methods, such as "platen interference"[17] on specimen deformation, and problems in maintaining uniformity of applied stresses across the faces of a cubic sample, which would prohibit such tests from becoming routine.

(iii) The relatively complex nature of the experimental equipment, which from spatial considerations with regard to the loading system, would prove difficult to adapt to permeability measurement.

Ideally, what is required for realistic strength, deformation and fluid flow measurements under realistic 3-D reservoir stresses, is the ability to subject small-diameter *cylindrical core plugs* to true triaxial stress fields, but by means of a *simple experimental facility* as relatively straightforward to operate as that used in axisymmetric triaxial testing. To this end, the following *true triaxial cell* has been designed, fabricated, proved and patented by the Rock Mechanics Group within the Department of Petroleum Engineering, Heriot-Watt University, with the specific intent of offering a new experimental facility to the oil industry.

## THE NEW TRUE TRIAXIAL CELL

### True Triaxial Cell Design

The true triaxial cell is as illustrated in Figure 1. Axial specimen loading is achieved through high strength 316-stainless steel platens, in an equivalent manner to the axisymmetric test, utilising a conventional stiff, servo-hydraulic compression machine. The body of the cell is composed of aluminium, which makes the rather bulky cell conveniently light to handle. The innovation lies in the application of radial pressure to the curved surface of a right circular cylindrical specimen 30mm in diameter with a length to diameter ratio of 2.25:1. This is developed in a stepwise manner, enabling an approximately elliptical radial stress distribution to be produced in the rock. As far as is known, this design is the only one capable of applying three independently variable principal stresses to a cylindrical core plug. Variation of the radial pressure is achieved by pressurising specially formed "trapped tubes", that is tubes which are aligned with the long axis of the specimen and are trapped between the curved surface of the specimen and the cell wall. Thus the trapped tubes develop the radial stresses on the rock core. These pvc tubes with initially circular cross-section are formed under heat to retain a flat face. Under pressure they expand, operating well above their rated unconfined burst capacity, while still being strong enough to withstand differences of up to at least 1000 psi (6.9 MPa) between adjacent tubes. The current design of cell utilises an array of 24 trapped tubes enabling pressures of up to 8000psi (55.2 MPa) to be developed before bursting, the ultimate aim being the development of radial stresses up to 10,000psi (68.9 MPa) in the specimen. A finite element comparative study of the stresses developed in the major principal plane of a conventional cubic specimen loaded under $\sigma_2 > \sigma_3$, and an equivalent loading generated by the true triaxial cell on a cylindrical specimen, showed that addition of a 3.5mm-thick Nitrile rubber liner in the latter produced an optimum, even distribution of the radial stresses.

Improvement of the cell technology has proceeded with the development of a more precise method for producing the deformed pvc tubing used to create the "trapped tubes". Previously the deformation was introduced after the tubes had been installed in the cell, by heating the cell and driving a tapered wedge through the space normally occupied by the core and its liner. The deformation is now produced by clamping the tubes in a heated mould which is then cooled. This provides a more accurate control over the geometry of the trapped tubes. The rubber liner which encapsulates the rock core is now mechanically compressed along its axis before applying pressure to the trapped tubes, creating a better seal between the core and the steel platens (of importance with

regard to permeability measurement) and preventing extrusion and bursting of the trapped tubes at high pressures.

### Multiple Servo-Control System

An affordable method of producing multiple servo-controlled hydraulic pressures for the array of trapped tubes has been devised with rapid response computer control and data logging. Servo-control is required on the tube pressures as volumetric strain in the rock core under testing can cause up to 30% deviation in the tube pressure when that pressure is applied with a hand pump. This is due to the high hydraulic stiffness of the trapped tube system. The method utilises servo-control valves which operate on air or nitrogen at 0-1MPa, driving a gas:oil 100:1 intensifier.

Current operation of the true triaxial cell utilises three independent servo-controlled hydraulic circuits, as shown in Figure 2, although there is no reason why this number could not be increased. Increasing the number of hydraulic circuits would enable the applied radial pressure to approximate more closely to a truly elliptical stress distribution. The total of 24 trapped tubes are divided into three banks of opposing 2 against 2, 4 against 4, and 6 against 6 tubes. The configuration illustrated shows hydraulic circuit No.1 applying $\sigma_2$ confining pressure to a total of 4 tubes, and circuit No.3 applying $\sigma_3$ confining pressure to a total of 12 tubes. Hydraulic circuit No.2 is shown applying a confining pressure intermediate between $\sigma_2$ and $\sigma_3$, to a total of 8 tubes. This enables the differential pressure between hydraulic circuits No.1 and No.3 to be effectively doubled to around 2000psi (13.8MPa), without the risk of tubes bursting. The whole pneumatic-hydraulic servo-control system for the true triaxial cell is trolley-based for manoeuvrability. Stainless steel 1/8"-diameter tubing with Swagelock fittings connects the cell hydraulic circuits to their independent servo-systems. A schematic of the servo-support for a single hydraulic circuit in the true triaxial cell is shown in Figure 3. Currently, three such systems are employed for overall control of the triaxial cell circuits. The electronic control-unit (1) presents LCD values for tube pressure, tube volume and pneumatic pressure, and enables specific individual pressures for all three circuits to be "dialled-in". The hydraulic system is charged to a certain pressure using a hand pump (2). Individual shut-off valves allow each circuit to be set at a different pressure (3). Bleed taps for the three circuits allow the oil pressure to be fine-tuned (4). A nitrogen communal gas receiver (5) acts as a reservoir for the pneumatic pressure system. Electronic control enables a voltage proportional to the pneumatic pressure to be dialled up, which backs off each pneumatic-hydraulic piston (6) to a specified pressure. The servo-unit (7) controls on this pressure. Specimen dilatancy or contractancy causes an inverse volume change in the bounding trapped tube assembly. The servo-valve (6) can be controlled either manually, or remotely via rapid response computer control (8) to correct for any such deviations from the initial set pressures. On specimen dilatancy and corresponding tube contraction, an additional pneumatic back-pressure system comprising a servo-valve (9) and solenoid (10), provides a kick to assist in overcoming frictional forces on the piston seals, aiding it in advancing to compensate for hydraulic pressure increase. Transducers (11) monitor piston displacements which can be converted to hydraulic volume changes knowing the piston cross-sectional area. Additional feedback is provided from a pressure transducer (12) on the high pressure fluid side of the system. Piston displacements and hydraulic pressures are monitored on the computer, as well as axial load and displacement outputs from the compression rig.

## EXPERIMENTAL RESULTS

### Strength Results

In order to assess true triaxial cell performance, a series of dry discrete failure tests on 30mm-diameter plugs of Locharbriggs sandstone were conducted. The test programme was designed to investigate any potential influence that $\sigma_2$ might have on rock strength. For each discrete test, whilst the specimen was held under differential $\sigma_2$ and $\sigma_3$ radial confining pressures applied using the true triaxial cell and its trapped tube array, $\sigma_a$ was increased from some hydrostatic value to

dynamic shear failure and beyond using a stiff compression rig in the conventional way. Simultaneous data logging of compression rig axial load and displacement with true triaxial cell hydraulic circuit pressures and piston displacements, has allowed system performance to be assessed over the complete stress-strain curve. Locharbriggs sandstone is a red medium- to coarse-grained Rotliegend analogue with about 83% quartz, 16% feldspar and 1% haematite. Typical data is represented by Figures 4(a) to (d), which show respectively plots of axial stress and confining channel pressure, volume and volumetric microstrain for $\sigma_2-\sigma_3$ = 6MPa at constant $\sigma_3$ = 30MPa. For considerable strain hardening and softening prior to dynamic failure and frictional sliding (4a) it is evident that the computer has managed to control each individual channel pressure to within about 0.5MPa of its initial desired value (4b). The necessary hydraulic volume change (4c) can be converted to an approximate volumetric microstrain (4d) by considering that each of the trapped tubes acts on a specimen segment of known volume 1/24th. that of the initial specimen volume, and that each hydraulic circuit contains a different number of trapped tubes. From Figure 4d it is evident that whilst specimen dilatancy is occurring parallel to $\sigma_3$, active specimen contractancy is occuring simultaneously parallel to $\sigma_2$, suggesting that both compressional and extensional strain is occurring in separate quadrants within the specimen volume at the same time, separated by lines of zero strain. This may well have important implications with regard to radial permeability.

Fifteen Locharbriggs specimens were tested using the computer control and data acquisition system, nine with $\sigma_3$ = 10MPa and six with $\sigma_3$ = 30MPa. Differential confining pressures have ranged from $\sigma_2-\sigma_3$ magnitudes of zero to 12MPa for constant $\sigma_3$. Peak and residual strengths obtained from discrete failure testing in the true triaxial cell are shown in Figure 5 in $\sigma_1$ versus $\sigma_2$ stress space, from which it is evident that increasing $\sigma_2$ has a significant strengthening effect on both the ultimate fracture stress and the frictional sliding stress. In all cases, the induced macroscopic fracture was observed to have been orientated under the applied stress field generated by the true triaxial cell, such that the strike of the fault plane was parallel to $\sigma_2$, with the fracture slipping against the direction of least confinement, $\sigma_3$.

**Permeability Results**

Axial permeability measurements over the complete stress-strain curve were conducted in core plugs of Locharbriggs sandstone, for stress conditions of $\sigma_2 = \sigma_3$ = 30MPa and $\sigma_2$ = 42MPa > $\sigma_3$ = 30MPa for both refined oil and distilled water pore fluids. Each permeability measurement was made at approximately 10MPa axial stress increments. Figure 6 shows the results for the inert oil permeant, under conditions of uniform radial stress (6a) and differential confining pressure (6b). In both cases some permeability recovery is evident prior to a permeability decline which is seen to be much greater for the differential confining pressure test. Results for the chemically active water permeant also measured under conditions of uniform radial stress (6c) and differential confining pressure (6d) are shown for comparison. For the water tests no permeability recovery was evident as observed with the oil pore fluid. Instead permeability showed an almost linear decrease from hydrostatic stress to post-failure conditions (6c) and a strongly sigmoidal decline with increasing axial stress (6d). For both oil and water pore fluids, the magnitude of the permeability decrease was seen to be significantly greater for differential confining conditions than for uniform radial confinement.

## DISCUSSION

From the above inital results, it is evident that lateral stress anisotropy and the magnitude of the intermediate principal stress have first order effects upon the deformability, strength and permeability of a typical reservoir sandstone analogue.

Of the failure criteria conventionally applied to rock, only the von Mises[18] and the extended 3-D Griffith[19] predict that $\sigma_2$ has any effect on fracture strength. The former can be expressed in terms of a linear relation between octahedral normal and shear

stresses, whilst the latter can be expressed in terms of a linear relation between stress invariants. Transposition of the strength data represented in Figure 5 in terms of principal stresses at failure, into the appropriate coordinates for the above criteria, allows re-plotting of the true triaxial cell data to assess the relative applicability of the von Mises and extended Griffith equations. This data can also be compared with failure laws generated from conventional multi-failure state testing of Locharbriggs sandstone in an axisymmetric cell. Both conventional and true triaxial cell data produced linear relationships for these criteria, although the constants of proportionality in each case differed significantly depending on the testing method. Whilst the von Mises and extended Griffith equations appear equally valid for predicting failure under conditions of $\sigma_2=\sigma_3$, the von Mises criterion appears superior to the extended Griffith under polyaxial stress states. Current work is concentrating upon the derivation of a general failure law incorporating both fabric anisotropy and horizontal stress anisotropy, from data obtained by testing laminated specimens within the true triaxial cell.

The axial permeability measurements described using the true triaxial cell serve to highlight the crucial effect played by the applied stress state. Permeability change over the complete axial stress-strain curve for both chemically active (distilled water) and inert (refined mineral oil) permeants is seen to be highly sensitive as to whether the applied triaxial stress is axisymmetric or general polyaxial. Future work will concentrate on understanding such observations in terms of differences in progressive microstructural deformation occurring within the specimen, using microseismics as a diagnostic tool. Peripheral insrumentation including axially mounted P- and orthogonal S-wave transducers for seismic velocity measurement, combined with acoustic emission monitoring, will hopefully provide the link between observed permeability sensitivities to general triaxial stress states, and deformation processes such as anelastic pore closure, dilatancy and microcrack coalescence.

A "mark II" true triaxial cell has recently been constructed which offers the additional facility of measuring radial permeability in two orthogonal directions, thus enabling direct quantification of potential stress-induced permeability anisotropy.

## CONCLUSIONS

(i) A novel cell for applying true triaxial stress states to cylindrical core plugs has been designed and tested successfully.
(ii) An inexpensive servo-control system for the cell has also been manufactured "in-house," providing rapid response computer control and data acquisition.
(iii) Induced shear fractures are consistently orientated by the cell in accordance with the 3-D applied stress field.
(iv) Both intact fracture strength and frictional sliding strength show a strong dependency on the magnitude of the intermediate principal stress.
(v) The cell has been utilised to measure the axial permeability of core plugs under differential confining pressures.
(vi) Axial permeability variation with deviatoric stress shows a first-order sensitivity to lateral stress anisotropy.

The above conclusions reinforce the belief of the authors that the true triaxial cell has the potential to offer an inexpensive means of routinely testing core plugs under general 3-D stress states, allowing efficient evaluation of both stress and permeability anisotropy for improved planning, exploitation and management of hydrocarbon reservoirs. In particular, the true triaxial cell has major application with regard to:

(i) Quantification of vertical to horizontal drainage ratios, $k_v/k_h$, for horizontal well evaluation.
(ii) Flood front migration and directional controls on pemeability and fracturing
(iii) Determination of $\sigma_H$ and $\sigma_h$ directions from the shear-wave acoustic extinction technique [20].

## NOMENCLATURE

$\sigma_1$: maximum principal stress
$\sigma_2$: intermediate principal stress
$\sigma_3$: minimum principal stress

$\sigma_v$: overburden stress
$\sigma_H$: maximum horizontal stress
$\sigma_h$: minimum horizontal stress
p: confining pressure
$\sigma_a$: axial stress
$k_v$: vertical permeability
$k_h$: horizontal permeability

## ACKNOWLEDGEMENTS

This work is funded by the Petroleum Science & Technology Institute of the U.K., and forms part of a continuing project studying, "The Combined Effects of Changes In Pore Fluid Chemistry and Stress State On Reservoir Permeability." The authors are grateful to PSTI staff and to members of the Industrial Steering Committee for their constructive comments. In particular, grateful thanks are extended to D. McLaughlin of Heriot-Watt University for his technical expertise in constructing the cell.

## REFERENCES CITED

[1] Hoek, E. & Franklin, J.A. 1968. A simple triaxial cell for field and laboratory testing of rock. *Trans. Inst. Min. Metall.*, London, Section A, Vol. 77, pp. 22-26.

[2] Franklin, J.A. & Hoek, E. 1970. Developments in triaxial testing equipment. *Rock Mechanics*, Vol. 2, pp. 223-228.

[3] Hoek, E. & Brown, E.T. 1980. *Underground Excavations In Rock.*. IMM, London, pp. 133-136.

[4] Brace, W.F. 1964. Brittle fracture of rocks. *In State of Stress In The Earth's Crust.* Judd, W.R. (ed.), Elsevier, N.Y., pp. 111-174.

[5] Hojem, J.M.P. & Cook, N.G.W. 1968. The design and construction of a triaxial and polyaxial cell for testing rock specimens. *South African Mech. Engr.*, Vol. 18, pp. 57-61.

[6] Wiebols, G.A. & Cook, N.G.W. 1968. An energy criterion for the strength of rock in polyaxial compression. *Int. J. Rock Mech. Min. Sci.*, Vol. 5, pp. 529-549.

[7] Mogi, K. 1970. Effect of triaxial stress system on rock failure. *Rock Mech. In Japan*, Vol. 1, pp. 53-55.

[8] Mogi, K. 1971. Fracture and flow of rocks under high triaxial compression. *J. Geophys. Res.*, Vol. 76, No. 5, pp. 1255-1269.

[9] Mogi, K. 1977. Dilatancy of rocks under general triaxial stress states with special reference to earthquake precursors. *J. Phys. Earth.*, 25, suppl.: S203-S217.

[10] Scholz, C.H. 1990. *The Mechanics of Earthquakes and Faulting.* Cambridge University Press, U.K. pp. 22-23.

[11] Gau, Q.Q., H.T. Cheng & D.P. Zhuo 1983. The strength, deformation and rupture characteristics of red sandstone under polyaxial compression. *Proc. 5th. Int. Cong. Rock Mech.*, Melbourne, Australia, Vol. A, pp. 157-160.

[12] Amadei, B. & Robison, J. 1986. Strength of rock in multi-axial loading conditions. *Proc. 27th. U.S. Symp. Rock Mech.*, Tuscaloosa, Alabama, pp. 47-55.

[13] Esaki, T. & Kimura, T. 1989. Mechanical behaviour of rocks under generalised high stress conditions. *Rock at Great Depth*, Maury, V. & Fourmaintraux, D., (eds.) Balkema, Rotterdam, Vol.1, pp.123-130.

[14] Sture, S. & Desai, C.S. 1979. Fluid cushion truly triaxial or multiaxial testing device. *Geotech. Testing J.*, 2: pp. 20-33.

[15] Jaeger, J.C. & Cook, N.G.W. 1979. *Fundamentals of Rock Mechanics* (3rd. Edn.) Chapman & Hall, London, pp.105-106.

[16] Handin, J., Heard, H.C. & Maguirk, J.N. 1967. Effects of the intermediate principal stress on the failure of limestone, dolomite and glass at different temperatures and strain rates. *J. Geophs. Res.*, Vol.72, pp. 611-640.

[17] Franklin, J.A. & Dusseault, M.B. 1989. *Rock Engineering* McGraw-Hill Inc., U.S.A., pp. 246-247.

[18] Mises, R. von. 1913. Mechanik der festen Körper im plastich deformablen Zustand, Nachr. Ges. Wiss. Göttingen, *Mathematisch-physikalische Klasse*, pp. 582-592.

[19] Murrell, S.A.F. 1963. A criterion for brittle fracture of rocks and concrete under triaxial stress and the effect of pore pressure on the criterion. Proc. 5th Rock Mech. Symp., Univ. of Minnesota. in *Rock Mechanics*, Fairhurst, C.(ed), Oxford Pergamon, pp. 563-577.

[20] Yale, D.P. & Sprunt, E.S. 1987. Prediction of fracture direction using shear acoustic anisotropy. *SCA Conference*, Paper Number 8711.

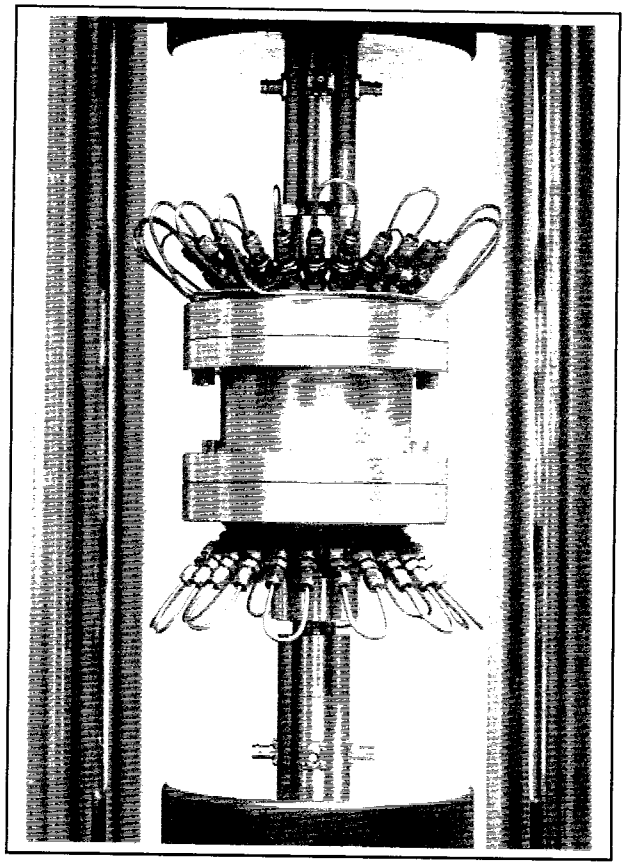

**Figure 1**

The true triaxial cell for the application of horizontal stress anisotropy, $\sigma_2 > \sigma_3$, sitting within a stiff compression rig applying $\sigma_1$ axially.

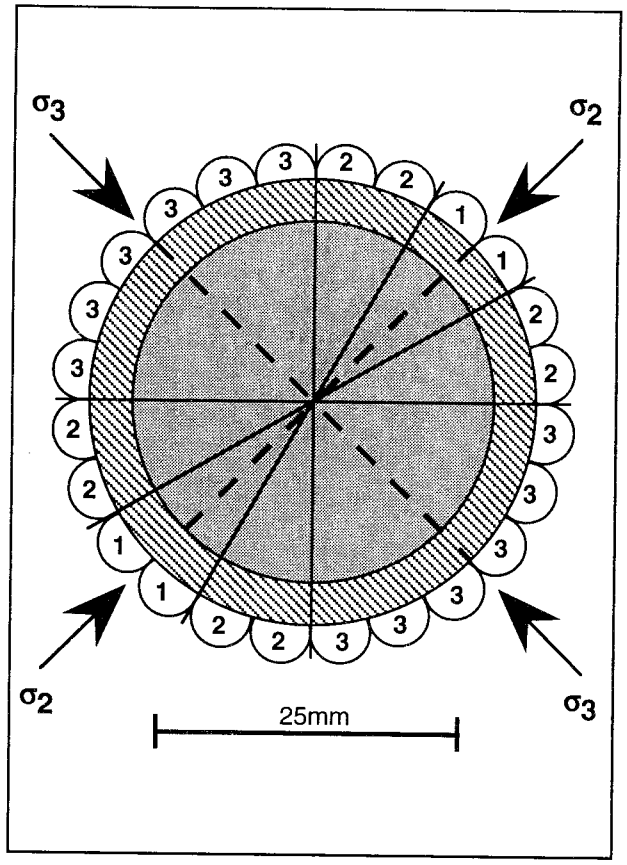


**Figure 2**

Cross-sectional plan view of the true triaxial cell showing independent servo-controlled hydraulic circuits 1, 2 & 3.

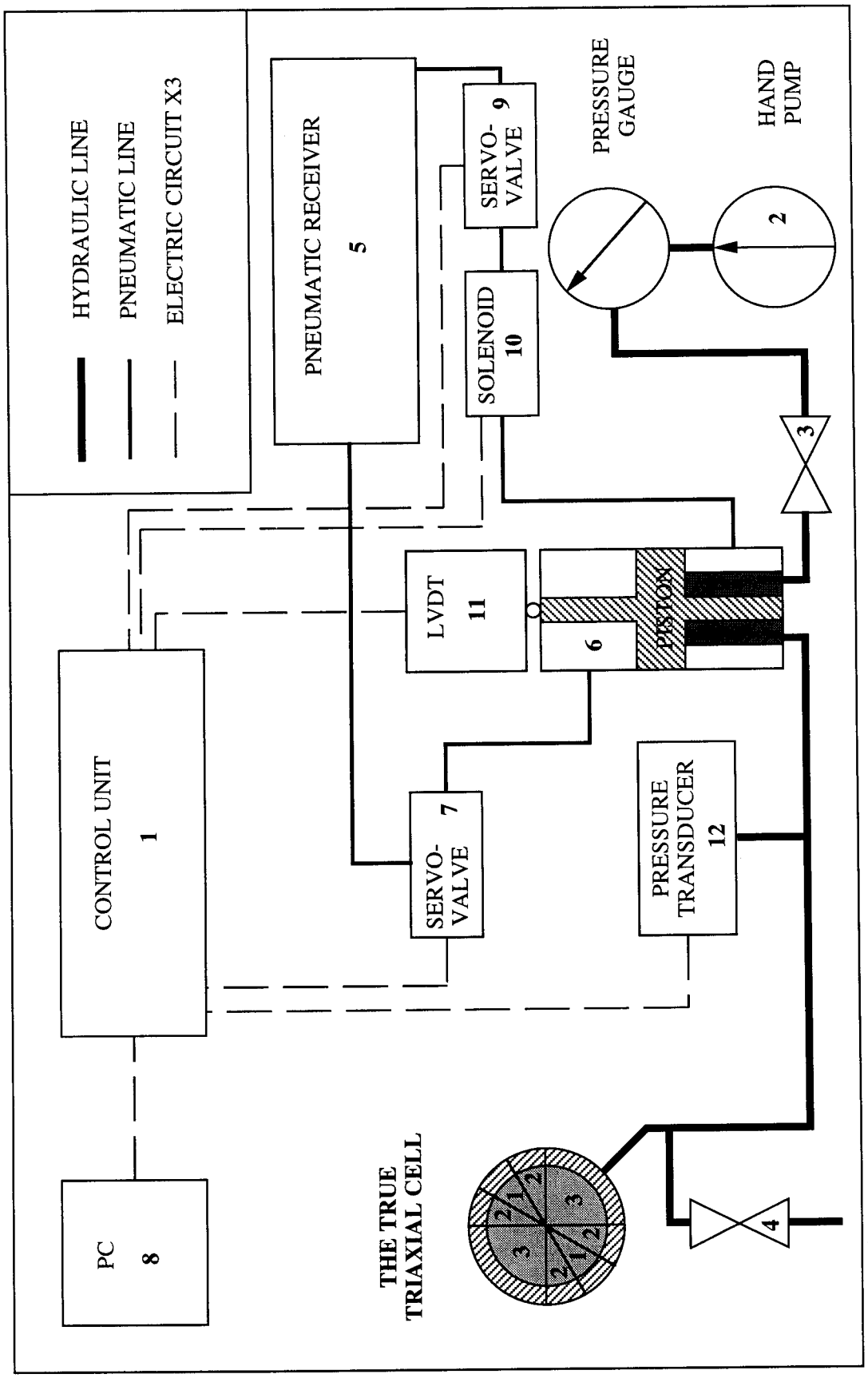


**Figure 3** Schematic of the pneumatic-hydraulic servo-control system for the true triaxial cell hydraulic circuits (see text for discussion).

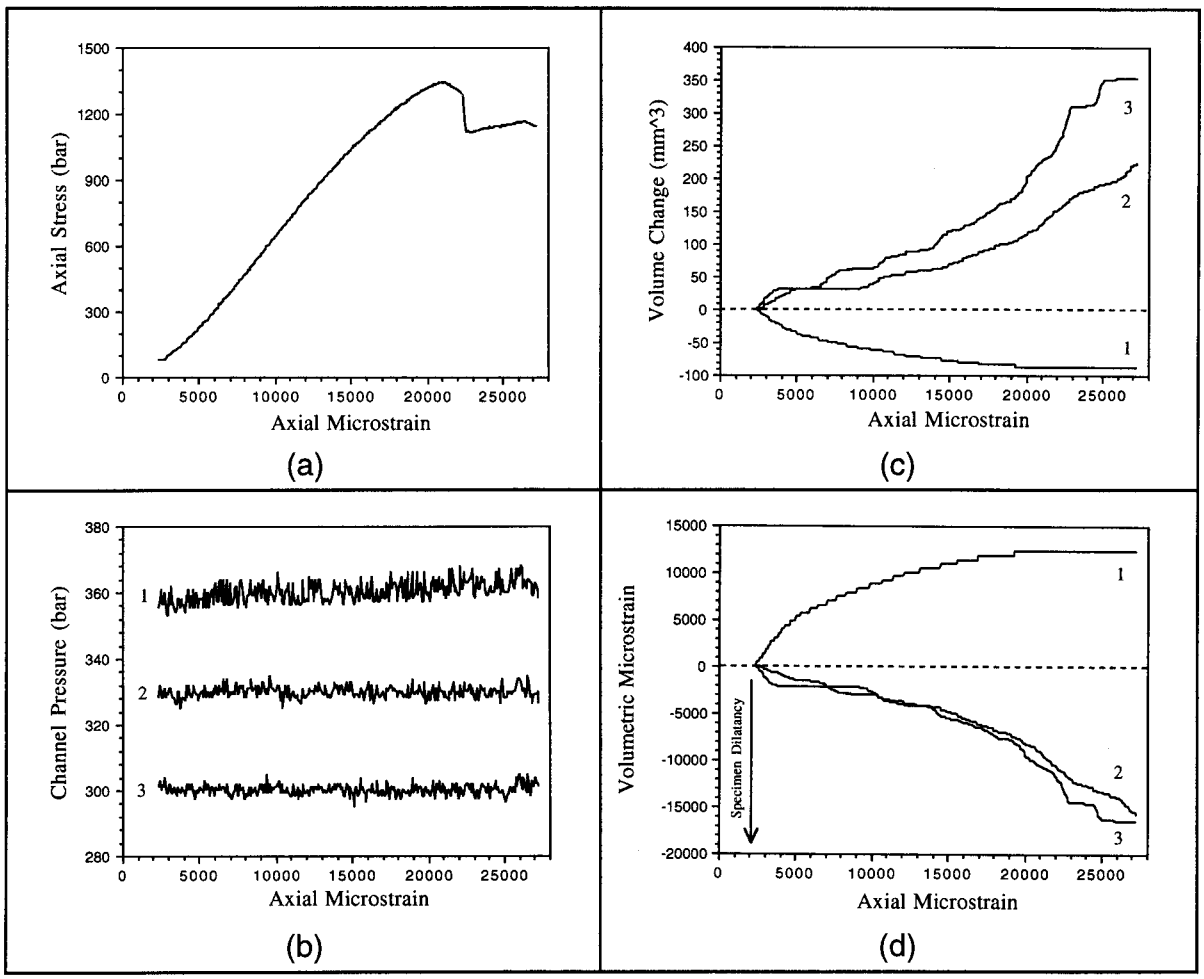


**Figure 4** Graphical output of computer logged data from true triaxial test

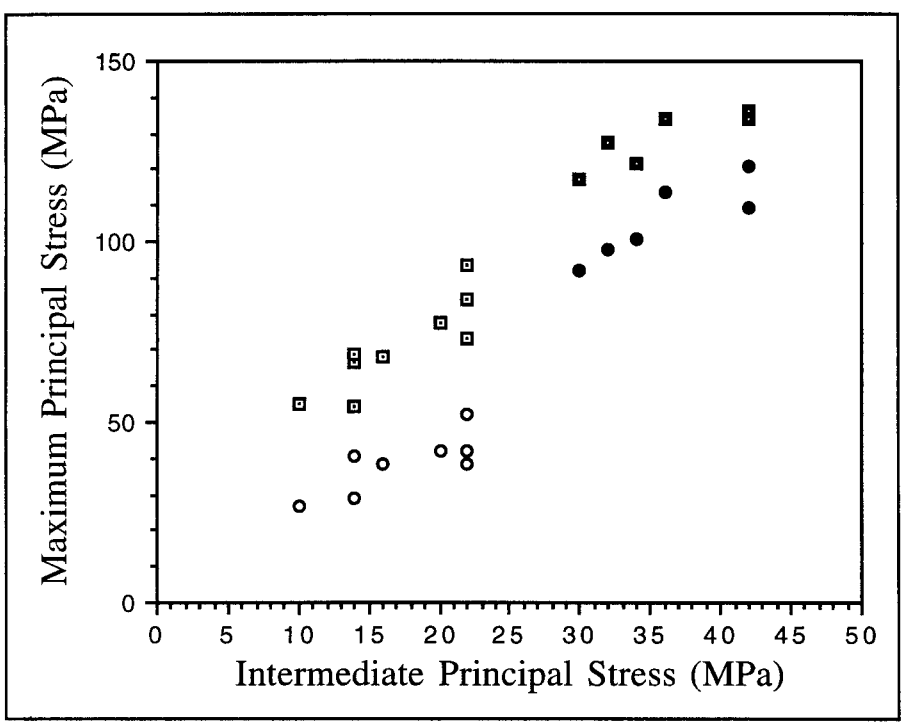


**Figure 5** The effect of $\sigma_2$ on strength. Open squares and circles represent peak and residual strengths respectively for constant $\sigma_3$ = 10MPa, filled squares and circles for $\sigma_3$ = 30MPa.

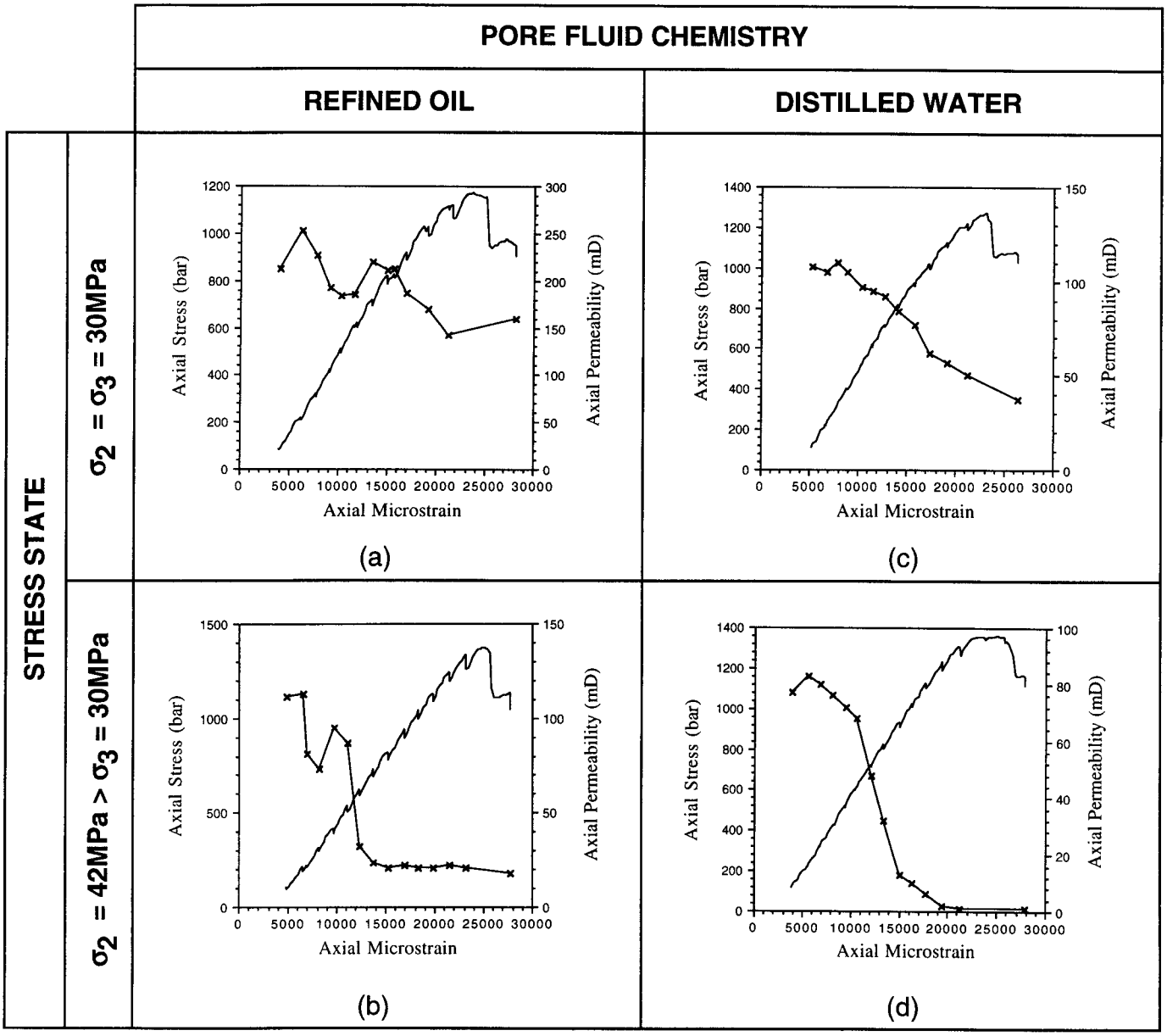


**Figure 6** Axial permeability variation over the complete stress strain curve as measured within the true triaxial cell.